Study on diffraction characteristics of a planar diamond waveguide

Xiuyun Ren (任秀云)[1], Zhaoshuo Tian (田兆硕)[1], Min Yang (杨 敏)[2], Yanfeng Zhang (张彦峰)[3], and Shiyou Fu (付石友)[1*]

[1]*Information Optoelectronics Research Institute, Harbin Institute of Technology at Weihai, Weihai 264209, China*

[2]*North China Sea Marine Technical Support Center, State Oceanic Administration, Qingdao 266033, China*

[3]*State Key Laboratory of Optoelectronic Materials and Technologies, School of Physics and Engineering, Sun Yat-sen University, Guangzhou 510275, China*

[*]*Corresponding author: fsytzs@126.com*

Received November 7, 2013; accepted December 19, 2013; posted online January 27, 2014

A numerical simulation is performed to study the far-field diffraction properties of planar diamond waveguides. The far-field intensity distributions of a planar air waveguide and a diamond waveguide with different distances are given by numerical calculations. In the experiment, the diffraction patterns on the screen with different distances are recorded using a He-Ne laser as the light source, wherein the laser beam is coupled with and propagates in the diamond waveguide. The simulation results are found to be consistent with the experimental ones.

OCIS codes: 230.7390, 070.7345, 220.2560, 260.6970.
doi: 10.3788/COL201412.022302.

The rapid developments in the field of integrated optoelectronics have led to the emergence of numerous optical waveguide devices with different functions and structures. These devices are extensively used in integrated optical circuits, high-power lasers, optical communication, and high-sensitivity optical monitoring[1−5]. A diamond waveguide has many significant optical properties and thus has potential applications in Raman lasers, quantum communication and computing, etc.[6,7]. Notably, fast and accurate numerical simulations are highly necessary in the design of optical waveguide devices because they have the advantages of high efficiency, low time consumption, low cost, and limitless analytical solutions. Numerical solutions can also provide the theoretical foundation for device designs and visually reflect the characteristics of optical waveguide devices. Some popular numerical simulation methods include the Couple–Mode theory[8], effective index method, finite element method[9,10], beam propagation based on the fast Fourier transform method, beam propagation based on the finite difference method[11], and finite difference time domain method[12,13]. The internal optical field distribution of the optical waveguide is usually simulated in all these methods, whereas the external optical field distribution of the optical waveguide is rarely considered. In practical applications such as in waveguide lasers, the optical beam propagation outside the optical waveguide is important. Thus, simulation of the far-field intensity distribution of the optical waveguide has great theoretical significance and provides guidance for potential applications.

In this letter, a planar air optical waveguide and a planar diamond waveguide are both theoretically and experimentally investigated. Diffraction theory in the frequency range is adopted to simulate the far-field diffraction properties of planar optical waveguides. In the experiments, the far-field diffraction patterns versus various distances are recorded using a camera. Comparison of the results of numerical simulations with experimental ones suggests that they are consistent. Therefore, this method is feasible for calculating the far-field intensity distribution of an optical planar waveguide.

The ideal planar waveguide structure is shown in Fig. 1. It consists of three layers, i.e., substrate, intermediate layer, and cladding, shaped into a sandwich structure. The refractive indices are n_1 with thickness a for the intermediate layer, n_2 for the substrate, and n_3 for the cladding. The longitudinal width (x-direction) of the planar waveguide is much larger than the thickness a and the light wavelength. Thus, the waveguide width can be taken as infinite. Generally, the light beam coupled with the end face of the waveguide is confined to the intermediate layer by total internal reflection. Therefore, a planar air waveguide can be formed by two reflectance mirrors with highly reflective coatings. The typical experimental installation used to study the far-field diffraction characteristics of a planar waveguide is shown in Fig. 2. The laser propagates along the z-axis; the plane coordinates of the entrance and exit of the planar waveguide are (x_1, y_1) and (x_2, y_2), respectively, and the plane coordinates of the screen are (x_3, y_3). The incident laser beam is focused onto the entrance of the planar waveguide using a lens and then passed through a planar waveguide cavity with length l. The light intensity distribution is shown on the screen located at a distance d from the end of the waveguide.

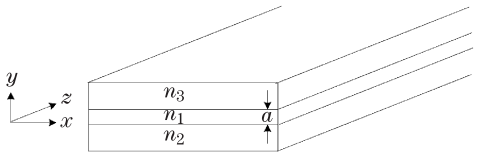

Fig. 1. Ideal planar waveguide structure.

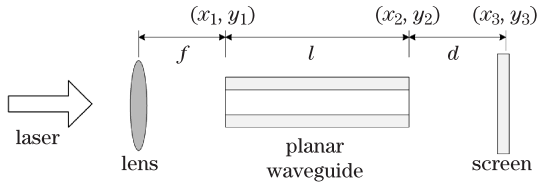

Fig. 2. Typical installation for studying the far-field diffraction of the planar waveguide.

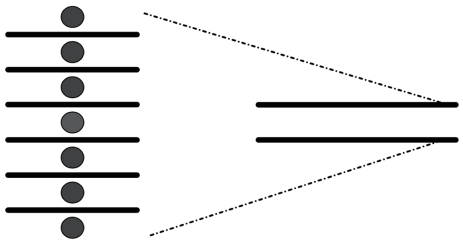

Fig. 3. Schematic of the equivalent light propagation for the planar waveguide.

Figure 3 shows the equivalent light propagation for the planar waveguide. Given the internal reflection between the two surfaces of the waveguide, the light field at the waveguide exit can be equivalent to the combination of many incident laser beams. Assuming that the number of light beams reflected by the two surfaces of the waveguide is $2N$, then the light field on the screen can be considered as the diffraction combination of $2N+1$ laser beams with different vertical positions passing through the waveguide[14].

The parallel incident laser rays converge to a Gauss beam with ω_0 waist radius at the entrance center of the planar waveguide. The complex amplitude of the light field can be written as $U_{(x_1,y_1)} = A\exp\left(-\frac{x_1^2+y_1^2}{\omega_0^2}\right)$, where A is the amplitude constant. The equivalent vertical coordinate of the reflection image in the (x_1, y_1) plane is $y_{1m} = mn_1a$, where a is the thickness of the planar waveguide, n_1 is the refractive index of the intermediate layer, and m *is* the order of reflection. Therefore, the normalized complex amplitude distribution in the planar waveguide exit plane (x_2, y_2) can be written as

$$U_m(x_2,y_2) = \left(\frac{2}{\pi\omega_0^2}\right)^{1/4} \exp\left[-\frac{x_2^2+(y_2\pm mn_1a)^2}{\omega^2(l)}\right] \cdot \exp\left\{ik[l+\frac{x_2^2+(y_2\pm mn_1a)^2}{2R(l)}]\right\}, \quad (1)$$

where $\omega(l)$ is the section radius of the Gauss beam at the exit plane of the waveguide, and $R(l)$ is the curvature radius of the Gauss beam wavefront. Therefore,

$$\omega(l) = \omega_0\left[1+\left(\frac{\lambda l}{\pi\omega_0^2}\right)^2\right]^{\frac{1}{2}}, \quad (2)$$

$$R(l) = l\left[1+\left(\frac{\pi\omega_0^2}{\lambda l}\right)^2\right]. \quad (3)$$

The propagation function of the planar waveguide to light can be taken as $2N+1$ laser beams interfering and being diffracted by the exit slit of the waveguide. Thus, the transmitted complex amplitude can be written as

$$U_{2N+1}(x_2,y_2) = \mathrm{rect}\left(\frac{y_2}{a}\right) \times \sum_{-N}^{N}\left(\frac{2}{\pi\omega_0^2}\right)^{\frac{1}{4}} \cdot \exp\left[-\frac{x_2^2+(y_2\pm mn_1a)^2}{\omega^2(l)}\right] \cdot \exp\left[ik\left(l+\frac{x_2^2+(y_2\pm mn_1a)^2}{2R(l)}\right)\right]. \quad (4)$$

The light propagation process is the diffraction of electromagnetic waves in space. According to the diffraction theory of angular spectrum, the light propagation process in free space from the diffraction screen to the view screen in the frequency range is equivalent to passing through an ideal low-pass filter with a $1/\lambda$ radius. Therefore, the complex amplitude distribution of the light field in the view screen can be calculated as[14]

$$U(x_3,y_3) = F^{-1}\left\{F[U_{2N+1}(x_2,y_2)]\exp\left[ikd\sqrt{1-(\lambda f_x)^2-(\lambda f_y)^2}\right]\right\}, \quad (5)$$

where F and F^{-1} are the Fourier transform and inverse Fourier transform, respectively; k is the module of the wave vector, $k = 2\pi/\lambda$; d is the distance between the waveguide exit and the view screen. Therefore, the intensity distribution on the screen is

$$I(x_3,y_3) = |U(x_3,y_3)|^2. \quad (6)$$

To verify the correctness of this numerical simulation method, the far-field diffraction characteristics of the planar air waveguide are studied both by simulations and experiments. In the simulation using MATLAB, the following parameters are chosen: refractive index of the air layer, n_1=1; waveguide thickness, a = 220 μm; waveguide length, l=20 mm; laser wavelength, λ=632.8 nm; waist radius of laser beam at the waveguide entrance, ω_0 = 25 μm. Figures 4(a) and (b) show the simulation results of the far-field diffraction intensity distributions of the planar air waveguide for d=60 and 90 mm, respectively. Results show that diffraction and interference induce changes in the far-field diffraction patterns compared with the incident Gauss beam, thereby forming

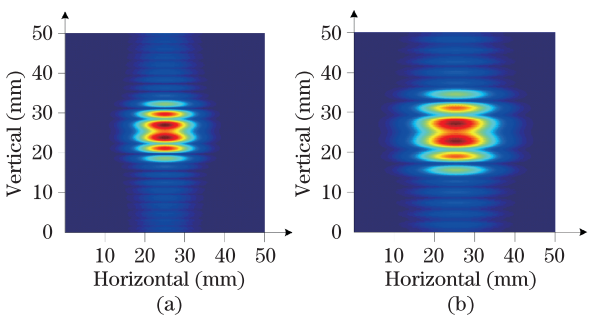

Fig. 4. (Color online) Simulation results of the far-field diffraction intensity distributions of the planar waveguide: (a) d=60 mm and (b) d=90 mm.

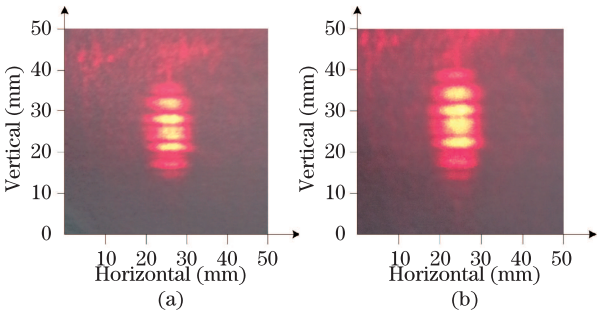

Fig. 5. (Color online) Experimental results of the far-field diffraction patterns of the planar air waveguide: (a) d=60 mm and (b) d=90 mm.

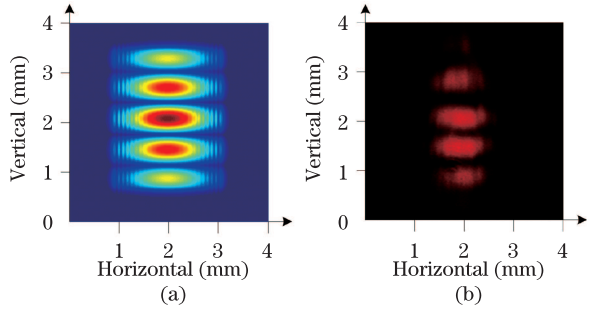

Fig. 6. (Color online) (a) Simulation and (b) experimental results of the far-field diffraction pattern of the planar diamond waveguide.

four central peaks with strong intensities and a number of sub-maxima with weaker intensities on both sides. Comparison of Figs. 4(a) and (b) reveals that the diffraction pattern remains nearly unchanged with increased diffraction distance, but the pattern size is somewhat expanded.

In the experiment, a planar air waveguide is formed by two pieces of space-adjustable reflectance mirrors with highly reflective coatings. The longitudinal width (x-direction) of the waveguide is 10 mm, and the waveguide length and thickness are chosen to have the same sizes as the simulation parameters. The waveguide can be equivalent to an infinite planar waveguide because the waveguide longitudinal width is much greater than the thickness and light wavelength. The He-Ne laser beam is focused by a converging lens with a focal length of 5 cm, and the waist radius at the entrance of the waveguide is measured to be $\omega_0 = 25$ μm using the knife-edge method.

Figures 5(a) and (b) show the corresponding experimental results of the diffraction patterns containing four central peaks with strong intensity and a number of sub-maxima with weaker intensities. Obviously, the simulation results agree with the experimental ones.

The far-field diffraction characteristics of the planar diamond waveguide are also studied both by simulation and experiment. In this MATLAB simulation, the parameters are chosen based on the diamond waveguide we have: the refractive index of diamond (intermediate layer) and SiO_2 (substrate) are n_1= 2.41 and n_3=1.46, respectively. The upper cladding is air, the waveguide thickness is $a = 14.4$ μm, and the waveguide length is l=2 mm. The other parameters are set as follows: laser wavelength, λ=632.8 nm; waist radius of laser beam at the waveguide entrance, $\omega_0 = 6$ μm. Figure 6(a) shows the simulation result of the far-field diffraction intensity distribution of the planar diamond waveguide at d=40 mm. The far-field diffraction pattern consists of five peaks with different intensities. Figure 6(b) presents the corresponding experimental results. Comparison of Figs. 6(a) and (b) reveals that the simulation results are consistent with the experimental ones.

In conclusion, numerical simulation based on diffraction theory in the frequency range is performed to study the far-field diffraction characteristics of a planar waveguide. The diffraction light intensity distributions of the planar air guide and planar diamond guide on the screen are numerically simulated using MATLAB. To verify the correctness of simulation results, a He-Ne laser beam is focused using a converging lens and then passed through the plane waveguide. Subsequently, the far-field diffraction patterns on the screen are experimentally measured. Comparisons are made between the simulation and experimental results, and both are found to be consistent.

This work was supported by the National Natural Science Foundation of China (No. 41306092), the Science and Technology Planning of Shandong Province, China (No. 2011GHY11514), and the Fundamental Research Funds for the Central Universities (Nos. HIT. BRET. 2010014 and HIT.NSRIF.2013139).

References

1. H. Cai, and A. W. Poon, Opt. Lett. **37,** 3000 (2012).
2. J. J. Plant, P. W. Juodawlkis , R. K. Huang, J. P. Donnelly, L. J. Missaggia, and K. G. Ray, IEEE Photon. Technol. Lett. **17,** 735 (2005).
3. J. A. Xia, A. M. Rossi, and T. E. Murphy, Opt. Lett. **37,** 256 (2012).
4. Y. Yan, C. Zheng, X. Sun, F. Wang, and D. Zhang, Chin. Opt. Lett. **10,** 092501 (2012).
5. H. Wu, L. Jiang, H. Li, W. Jia, G. Zheng, H. Qiang, and X. Li, Chin. Opt. Lett. **9,** 011301 (2011).
6. Y. F. Zhang, L. McKnight, Zh. Sh. Tian, S. Calvez, and M. D. Dawson, Diamond Relat. Mater. **20,** 564 (2011).
7. D. Sage, L. M. Pham, N. Bar-Gill, C. Belthangady, M. D. Lukin, A. Yacoby, and R. L. Walsworth, Phys. Rev. B **85,** 121202 (2012).
8. E. Marcatili, IEEE J. Quantum Electron. **22,** 988 (1986).
9. D. Sun, J. Manges, X. C. Yuan, and Z. Cendes, IEEE Trans. Antennas Propag. **37,** 12 (1995).
10. S. S. A. Obayya, IEEE J. Quantum Electron. **40,** 591 (2004).
11. M. A. Swillam, M. H. Bakr, and X. Li, J. Lightwave Technol. **25,** 1861 (2007).
12. M. Ali and S. Sanyal, Prog. Electromagn. Res. **2,** 291 (2008).
13. L. Huang, B. Chen, Y. Li, and C. Liu, Chin. Opt. Lett. **10,** 011301 (2012).
14. J. C. Li, *Diffraction of Laser and Calculation on Thermal Acting* (Science Press, Beijing, 2008)